# A Multispecies Pseudoadiabat for Simulating Condensable-rich Exoplanet Atmospheres

R. J. Graham ⬤, Tim Lichtenberg ⬤, Ryan Boukrouche ⬤, and Raymond T. Pierrehumbert ⬤
Atmospheric, Oceanic and Planetary Physics, Department of Physics, University of Oxford, UK; robert.graham@physics.ox.ac.uk
*Received 2021 March 18; revised 2021 August 22; accepted 2021 August 24; published 2021 October 6*

## Abstract

Central stages in the evolution of rocky, potentially habitable planets may play out under atmospheric conditions with a large inventory of nondilute condensable components. Variations in condensate retention and accompanying changes in local lapse rate may substantially affect planetary climate and surface conditions, but there is currently no general theory to effectively describe such atmospheres. In this article, expanding on the work by Li et al., we generalize the single-component moist pseudoadiabat derivation in Pierrehumbert to allow for multiple condensing components of arbitrary diluteness and retained condensate fraction. The introduction of a freely tunable retained condensate fraction allows for a flexible, self-consistent treatment of atmospheres with nondilute condensable components. To test the pseudoadiabat's capabilities for simulating a diverse range of climates, we apply the formula to planetary atmospheres with compositions, surface pressures, and temperatures representing important stages with condensable-rich atmospheres in the evolution of terrestrial planets: a magma ocean planet in a runaway greenhouse state; a post-impact, late-veneer-analog planet with a complex atmospheric composition; and an Archean Earth-like planet near the outer edge of the classical circumstellar habitable zone. We find that variations in the retention of multiple nondilute condensable species can significantly affect the lapse rate and in turn outgoing radiation and the spectral signatures of planetary atmospheres. The presented formulation allows for a more comprehensive treatment of the climate evolution of rocky exoplanets and early Earth analogs.

*Unified Astronomy Thesaurus concepts:* Planetary atmospheres (1244); Atmospheric composition (2120); Astrobiology (74); Exoplanet structure (495)

## 1. Introduction

The vertical temperature structure of an atmosphere is a primary determinant of planetary climate and surface evolution. The temperature gradient in convecting regions of atmospheres can generally be described by some form of adiabat (in the reversible case) or pseudoadiabat (in the irreversible case) that models the expansion and cooling of parcels of air as they are buoyed upward. In the case where none of the gases in the atmosphere can condense at the local temperature and pressure, the atmosphere follows a "dry adiabat," where the temperature profile is determined entirely by the cooling of a convecting parcel as it expands and does work on its surroundings. In the case where the atmosphere is composed of a dry component mixed with "wet" components that can condense under the local temperature/pressure conditions, the latent heat released by condensation partially offsets the cooling by expansion work, leading to a "moist adiabat" with a lapse rate that is less steep than would be the case under dry conditions.

Moist adiabats and pseudoadiabats with one (e.g., Ingersoll 1969; Pierrehumbert 2010) or recently multiple (Li et al. 2018) condensables have been derived and used to investigate planetary atmospheres with a range of compositions. Ingersoll (1969) exploited entropy conservation to derive both an adiabat (with all condensate retained in the column) and a pseudoadiabat (with instantaneous rainout of all condensate) to describe atmospheres with a single nondilute condensable component in the context of modeling Venus undergoing a runaway greenhouse effect. Li et al. (2018) took the same entropy-based approach to derive a fully reversible, condensate-retaining

moist adiabat with multiple condensing components to describe the atmospheres of gas giant planets. An alternate approach to the derivation of moist (pseudo)adiabats is to begin with a statement of energy conservation. Weidenschilling & Lewis (1973) used energy conservation to derive a single-component moist pseudoadiabat to model the Jovian planets, and Pierrehumbert (2010) took the same approach during a pedagogical discussion of atmospheric thermodynamics.

Here, we apply the energy conservation approach to derive a lapse rate formula that allows for multiple condensing components and the specification of arbitrary retained condensate fractions. For atmospheres with dilute condensable components, regardless of retained condensate fraction, the temperature–pressure profiles produced by this formula differ negligibly from those produced by the fully reversible adiabat derived in Li et al. (2018). However, under nondilute conditions, the retained condensate fraction controls the effective specific heat of the atmosphere, which in turn strongly influences the lapse rate of the atmosphere. With the assumption of complete condensate retention that is made in Li et al. (2018), nondilute atmospheres develop upper atmospheres composed almost entirely of condensate, with gas at times making up less than 1% of moles at low pressures/temperatures where nearly all of the gas has condensed. When the ratio of gas to condensate is very small, a change in the temperature of a mole of the gas also requires changing the temperature of many moles of a solid/liquid phase, effectively increasing the specific heat capacity of the gas and making its temperature less sensitive to expansion work done on the surroundings. It is unclear how realistic that situation might be, so it is important to be able to vary the degree of condensate retention when modeling exotic atmospheres with nondilute condensable components.

We derived the following lapse rate equation to deal with this issue explicitly:

$$\frac{d \ln T}{d \ln P}$$

$$= \frac{x_d + \sum_i x_{v,i}}{x_d \frac{c_d x_d + \sum_i (x_{v,i}(c_{v,i} - R\beta_i + R\beta_i^2) + \alpha_i x_{c,i} c_{c,i})}{R(x_d + \sum_i \beta_i x_{v,i})} + \sum_i \beta_i x_{v,i}}, \quad (1)$$

where $\frac{d \ln T}{d \ln P}$ is the lapse rate of temperature $T$ with respect to total pressure $P$; $x_{\{\}}$ is the mole fraction of a dry gas component (or gas mixture) ($x_d$), a condensable vapor component ($x_{v,i}$), or a condensate component ($x_{c,i}$); $c_{\{\}}$ is the molar specific heat at constant pressure [J K$^{-1}$ mol$^{-1}$] of a dry gas/mixture ($c_d$), a condensing gas ($c_{v,i}$), or a condensate ($c_{c,i}$); $R = 8.314$ [J K$^{-1}$ mol$^{-1}$] is the universal ideal-gas constant; $\beta_i = \frac{L}{RT}$, where $L$ [J mol$^{-1}$] is the latent heat of condensable component $i$; and $\alpha_i$ is the mole fraction of condensate that is retained in the column instead of raining out for species $i$. It is important to note that the mole fractions $x_{\{\}}$ in this equation obey the relation $x_d + \sum_i x_{v,i} + \sum_i x_{c,i} = 1$, and that $x_{c,i}$ is the total condensate produced in a given parcel of air during its ascent from the surface, including both retained ($\alpha_i x_{c,i}$) and rained-out ($(1 - \alpha_i)x_{c,i}$) components. The mole fractions of components *in the atmosphere* can be calculated with $X_{\{\}}^i = \frac{x_{\{\}}}{1 - (1 - \alpha_i)x_{c,i}}$ for the gaseous components and $X_c^i = \frac{\alpha_i x_{c,i}}{1 - (1 - \alpha_i)x_{c,i}}$ for the condensate components.

This pseudoadiabat can be applied to model a very broad range of atmospheric compositions. To illustrate this, we use the formula to explore several scenarios where condensable components may dominate terrestrial atmospheres: (i) a magma ocean (MO) planet with a partially molten surface, (ii) an impact-induced, transiently reducing atmosphere during the late veneer (LV), and (iii) the atmosphere of an Earth-like planet in the early stages of its habitable phase, with high CO$_2$ partial pressure and temperate surface climate. Each case has at least one abundant condensable species, so the degree of condensate retention is an especially important consideration in calculating temperature structure of these atmospheres. Previous work on atmospheres with nondilute condensable components has demonstrated that these planets exhibit globally weak temperature gradients regardless of spin state (Pierrehumbert & Ding 2016; Ding & Pierrehumbert 2018), suggesting that one-dimensional atmospheric column models are a useful tool for exploring the properties of these atmospheres.

The paper is structured as follows. In Section 2 we derive the adiabat formula. Readers mainly interested in the main features of the adiabat, and less in the derivation itself, may continue in Section 2.3 and following, where we illustratively point out and discuss the influence on the lapse rate and condensation. In Section 3 we demonstrate the impact of the retained condensate fraction on atmospheric structure and radiative transport for the three reference scenarios mentioned in the previous paragraph. In Section 4 we discuss the relevance for exoplanet atmospheres and the near-surface evolution of prebiotic Earth and highlight some caveats with our analysis. We summarize and conclude in Section 5.

## 2. Multicomponent Pseudoadiabat

### 2.1. Derivation

In this section, we derive the formula for the multi-condensable moist pseudoadiabat from basic thermodynamic principles. Readers with less interest in the mathematical derivation may skip to Section 2.3 to see the application of the formula to condensable-rich atmospheres. This derivation is a generalization of the single-component pseudoadiabat derivation presented in Section 2.7.2 of Pierrehumbert (2010). We begin with a statement of the first law of thermodynamics for a parcel of gas with $n_d$ moles of noncondensable substance, $\sum_i n_{v,i}$ moles of vapor of condensable substance, and $\sum_i \alpha_i n_{c,i}$ moles of condensate, where $n_{c,i}$ is the total number of moles of substance $i$ that have condensed over the history of the parcel and $\alpha_i \in [0,1]$ is the fraction of condensate $i$ that has been retained in the parcel. The subscript $i$ iterates over the number of condensable species, and the subscript $d$ represents the noncondensable ("dry") phase, which may actually be the molar mean of arbitrarily many dry phases. If temperature, noncondensable pressure, and condensable pressure are changed, respectively, by infinitesimal increments $dT$, $dP_d$, and $\sum_i dP_i$, enthalpy conservation for the parcel can be stated as

$$\left(n_d + \sum_i (n_{v,i} + \alpha_i n_{c,i})\right)\delta Q$$
$$= n_d c_d dT - V_d dP_d$$
$$+ \sum_i (n_{v,i} c_{v,i} dT + \alpha_i n_{c,i} c_{c,i} dT - V_i dP_i + L_i dn_{v,i}) \quad (2)$$

$$\left(n_d + \sum_i (n_{v,i} + \alpha_i n_{c,i})\right)\delta Q$$
$$= n_d c_d dT - n_d RT \frac{dP_d}{P_d}$$
$$+ \sum_i \left(n_{v,i} c_{v,i} dT + \alpha_i n_{c,i} c_{c,i} dT\right.$$
$$\left. - n_{v,i} RT \frac{dP_i}{P_i} + L_i dn_{v,i}\right), \quad (3)$$

where $\delta Q$ is the change in total energy per mole of the parcel (=0 if the parcel is an energetically closed system, as we will assume), the $-VdP$ terms represent the work done to change pressures, the second line comes from the ideal-gas law $\left(V = \frac{nRT}{P}\right)$, $R$ is the universal gas constant [J K$^{-1}$ mol$^{-1}$], $L_i$ is the molar latent heat for each condensable species [J mol$^{-1}$], and $dn_{v,i}$ represents the change in number of moles of each condensable substance due to condensation.

Next, we set $\delta Q = 0$, divide the equation by $n_d T$, and define $\eta_{v,i} = \frac{n_{v,i}}{n_d}$:

$$0 = c_d \frac{dT}{T} - R\frac{dP_d}{P_d}$$
$$+ \sum_i \left(\frac{n_{v,i}}{n_d}c_{v,i}\frac{dT}{T} + \alpha_i \frac{n_{c,i}}{n_d}c_{c,i}\frac{dT}{T}\right. \quad (4)$$
$$\left. - \frac{n_{v,i}}{n_d}R\frac{dP_i}{P_i} + \frac{L_i dn_{v,i}}{n_d T}\right)$$

$$=c_d\frac{dT}{T} - R\frac{dP_d}{P_d} + \sum_i \left( \eta_{v,i}c_{v,i}\frac{dT}{T} \right.$$
$$\left. + \alpha_i\eta_{c,i}c_{c,i}\frac{dT}{T} - \eta_{v,i}R\frac{dP_i}{P_i} + \frac{L_i}{T}d\eta_{v,i} \right) \tag{5}$$

where $\eta_{\{\},i}$ is the molar mixing ratio of condensable or condensate species $i$ with the noncondensable gas.

Next, we rewrite $d\eta_{v,i}$ in terms of changes to pressure and make use of the fact that the condensable pressures follow the ideal-gas form of the Clausius–Clapeyron equation (see Equation (11)) to rewrite $\frac{dP_i}{P_i}$ in terms of a change to the temperature (we note that application of this form of the Clausius–Clapeyron equation implies the assumption that the specific volume of the condensate phase being described is negligible compared to that of the vapor phase of the same species–this assumption begins to break down near the critical point where gas and liquid phases become indistinguishable, so in some high-temperature and/or high-pressure atmospheres, the accuracy of the pseudoadiabat will be reduced):

$$d\eta_{v,i} = d\left(\frac{P_i}{P_d}\right) \tag{6}$$

$$= \frac{P_i}{P_d}d\ln\left(\frac{P_i}{P_d}\right) \tag{7}$$

$$= \eta_{v,i}(d\ln(P_i) - d\ln(P_d)) \tag{8}$$

and

$$P_i = P_{sat,i}(T) \tag{9}$$

$$\frac{dP_i}{P_i} = d\ln P_i = \frac{d\ln(P_{sat,i}(T))}{dT}dT \tag{10}$$

$$= \frac{L_i}{RT^2}dT \tag{11}$$

$$= \frac{L_i}{RT}d\ln T, \tag{12}$$

both of which can now be substituted into the statement of the first law,

$$0 = c_d d\ln T - Rd\ln P_d + \dots$$
$$\sum_i \left( \eta_{v,i}c_{v,i}d\ln T + \alpha_i\eta_{c,i}c_{c,i}d\ln T \right.$$
$$\left. - \eta_{v,i}\frac{L_i}{T}d\ln T + \frac{\eta_{v,i}L_i}{T}\left(\frac{L_i}{RT}d\ln T - d\ln P_d\right) \right) \tag{13}$$

which now only has differentials of $\ln P_d$ and $\ln T$. We can now gather terms with each differential,

$$d\ln P_d\left(R + \sum_i \frac{\eta_{v,i}L_i}{T}\right)$$
$$= d\ln T\left(c_d + \sum_i\left(\eta_{v,i}\left(c_{v,i} - \frac{L_i}{T} + \frac{L_i^2}{RT^2}\right)\right.\right.$$
$$\left.\left. + \alpha_i\eta_{c,i}c_{c,i}\right)\right), \tag{14}$$

and solve for $\frac{d\ln T}{d\ln P_d}$,

$$\frac{d\ln T}{d\ln P_d}$$
$$= \frac{R + \sum_i \frac{\eta_{v,i}L_i}{T}}{c_d + \sum_i\left(\eta_{v,i}\left(c_{v,i} - \frac{L_i}{T} + \frac{L_i^2}{RT^2}\right) + \alpha_i\eta_{c,i}c_{c,i}\right)}, \tag{15}$$

which represents the lapse rate with respect to changes in the noncondensable component's pressure.

Now, to get the lapse rate with respect to changes to the total pressure, we note

$$\frac{d\ln T}{d\ln P} = \frac{d\ln T}{d\ln P_d}\frac{d\ln P_d}{d\ln P}, \tag{16}$$

where $P = P_d + \sum_i P_i$.

So, the next step is to write $\frac{d\ln P_d}{d\ln P}$ in terms of convenient variables:

$$\frac{d\ln P_d}{d\ln P} = \frac{P}{P_d}\frac{dP_d}{dP} \tag{17}$$

$$= \frac{P_d + \sum_i P_i}{P_d}\left(\frac{dP_d}{d(P_d + \sum_i P_i)}\right) \tag{18}$$

$$= \left(1 + \sum_i\frac{P_i}{P_d}\right)\left(1 + \sum_i\frac{dP_i}{dP_d}\right)^{-1} \tag{19}$$

$$= \left(1 + \sum_i\frac{P_i}{P_d}\right)\left(1 + \sum_i\left(\frac{dP_i}{dT}\Big/\frac{dP_d}{dT}\right)\right)^{-1} \tag{20}$$

$$= \left(1 + \sum_i\eta_{v,i}\right)\left(1 + \sum_i\left(\frac{L_iP_i}{RT^2}\right)\right.$$
$$\left. \times \left(\frac{T}{P_d}\frac{d\ln T}{d\ln P_d}\right)\right)^{-1} \tag{21}$$

$$= \frac{1 + \sum_i\eta_{v,i}}{1 + \sum_i\frac{L_i}{RT}\eta_{v,i}\frac{d\ln T}{d\ln P_d}} \tag{22}$$

$$= \frac{x_d + \sum_i x_{v,i}}{x_d + \sum_i\beta_i x_{v,i}\frac{d\ln T}{d\ln P_d}}, \tag{23}$$

where $\beta \equiv \frac{L_i}{RT}$ and $x_{\{\}}$ represents the mole fraction of a substance, such that $\frac{x_{v,i}}{x_d} = \eta_{v,i}$.

Now we can write down $\frac{d\ln T}{d\ln P}$. We substitute $\frac{x_{v,i}}{x_d}$ for $\eta_{v,i}$ and multiply $x_d$ from the denominator to avoid dealing with $\eta_{v,i}$ going to infinity at vanishing noncondensable partial pressure, and we substitute $\beta_i$ for $\frac{L_i}{RT}$ for compactness:

$$\frac{d\ln T}{d\ln P} = \frac{d\ln P_d}{d\ln P}\frac{d\ln T}{d\ln P_d} \tag{24}$$

$$= \frac{x_d + \sum_i x_{v,i}}{x_d + \sum_i\beta_i x_{v,i}\frac{d\ln T}{d\ln P_d}}\frac{d\ln T}{d\ln P_d} \tag{25}$$

$$= \frac{x_d + \sum_i x_{v,i}}{x_d\left(\frac{d\ln T}{d\ln P_d}\right)^{-1} + \sum_i\beta_i x_{v,i}} \tag{26}$$

$$= \frac{x_d + \sum_i x_{v,i}}{x_d \frac{c_d x_d + \sum_i (x_{v,i}(c_{v,i} - R\beta_i + R\beta_i^2) + \alpha_i x_{c,i} c_{c,i})}{R(x_d + \sum_i \beta_i x_{v,i})} + \sum_i \beta_i x_{v,i}}, \quad (27)$$

which we later demonstrate to be equivalent to the reversible multicondensable adiabat derived in Li et al. (2018), with the fraction of retained condensate in that formula set equal to $\alpha$ instead of 1 (see Section 2.2).

It is simple to show that this formula yields reasonable answers at various limits. For example, the dry adiabat can be derived by setting $\sum_i x_{v,i} = \sum_i x_{c,i} = 0$ and $x_d = 1$ (e.g., assuming a column of noncondensable gas):

$$\left. \frac{d \ln T}{d \ln P} \right|_{\text{dry}}$$

$$= \frac{1 + \sum_i 0}{1 \times \frac{c_d \times 1 + \sum_i (0 \times (c_{v,i} - R\beta_i + R\beta_i^2) + \alpha_i \times 0 \times c_{c,i})}{R(1 + \sum_i \beta_i \times 0)} + \sum_i \beta_i \times 0}$$

$$(28)$$

$$= \frac{R}{c_d}, \quad (29)$$

which is the correct formula. Similarly, we can set $x_d = \sum_i \alpha_i x_{c,i} = 0$ to represent an atmosphere made entirely of condensing species with instantaneous rainout of condensates:

$$\left. \frac{d \ln T}{d \ln P} \right|_{\text{moist}} = \frac{\sum_i x_{v,i}}{\sum_i \beta_i x_{v,i}} \quad (30)$$

$$= \frac{1}{\sum_i \beta_i x_{v,i}}, \quad (31)$$

which yields the familiar Clausius–Clapeyron equation when evaluated with a single component, $\frac{d \ln T}{d \ln P}\big|_{CC} = \frac{1}{\beta} = \frac{RT}{L}$.

### 2.2. Convergence to Reversible Multicondensable Adiabat

Here we show that the multicondensable adiabat derived in Li et al. (2018) can be obtained by setting the fraction of retained condensate to 1 in the formula derived here:

$$\frac{d \ln T}{d \ln P}$$

$$= \frac{x_d + \sum_i x_{v,i}}{x_d \frac{c_d x_d + \sum_i (x_{v,i}(c_{v,i} - R\beta_i + R\beta_i^2) + \alpha_i x_{c,i} c_{c,i})}{R(x_d + \sum_i \beta_i x_{v,i})} + \sum_i \beta_i x_{v,i}} \quad (32)$$

$$= \frac{1 + \sum_i \eta_{v,i}}{\frac{c_d x_d + \sum (x_{v,i}(c_{v,i} - R\beta_i + R\beta_i^2) + \alpha_i x_{c,i} c_{c,i})}{R x_d (1 + \sum_i \beta_i \eta_{v,i})} + \sum_i \beta_i \eta_{v,i}} \quad (33)$$

$$= \frac{1 + \sum_i \beta_i \eta_{v,i}}{\frac{c_d x_d + \sum_i (x_{v,i} c_{v,i} + \alpha_i x_{c,i} c_{c,i})}{R(x_d + \sum_i x_{v,i})} + \frac{\sum_i (-\beta_i \eta_{v,i} + \beta_i^2 \eta_{v,i}) + \sum_i \beta_i \eta_{v,i} + \left(\sum_i \beta_i \eta_{v,i}\right)^2}{1 + \sum_i \eta_{v,i}}}$$

$$(34)$$

$$= \frac{1 + \sum_i \beta_i \eta_{v,i}}{\frac{c_d x_d + \sum_i (x_{v,i} c_{v,i} + \alpha_i x_{c,i} c_{c,i})}{R(x_d + \sum_i x_{v,i})} + \frac{\sum_i (\beta_i^2 \eta_{v,i}) + \left(\sum_i \beta_i \eta_{v,i}\right)^2}{1 + \sum_i \eta_{v,i}}} \quad (35)$$

$$= \frac{1 + \sum_i \beta_i \eta_{v,i}}{\frac{\widehat{c_p}}{R} + \frac{\sum_i (\beta_i^2 \eta_{v,i}) + \left(\sum_i \beta_i \eta_{v,i}\right)^2}{1 + \sum_i \eta_{v,i}}}, \quad (36)$$
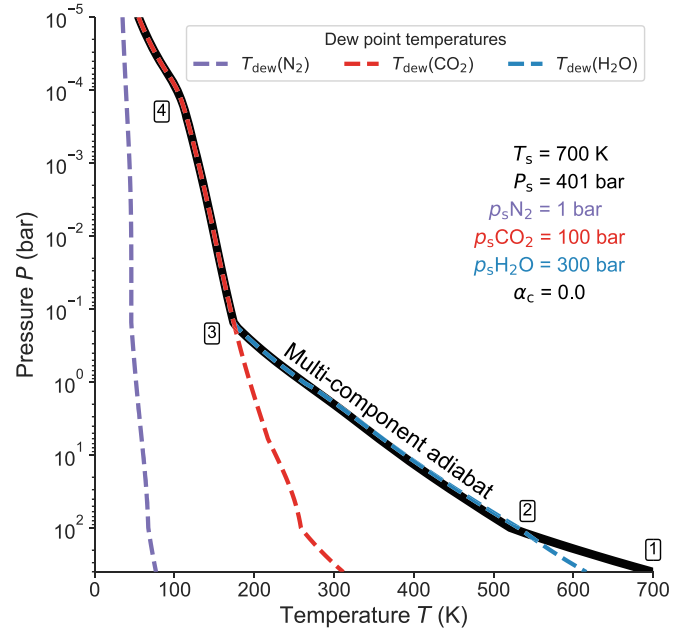


**Figure 1.** Annotated illustration of some basic adiabat features in a hypothetical $N_2$–$CO_2$–$H_2O$ atmosphere with a surface temperature of 700 K. See main text for discussion.

where $\widehat{c_p} = \frac{c_d x_d + \sum_i (x_{v,i} c_{v,i} + \alpha_i x_{c,i} c_{c,i})}{(x_d + \sum_i x_{v,i})}$. This is identical to Equation (1) in Li et al. (2018), except that the $\widehat{c_p}$ in their Equation (1) has $\alpha_i = 1$, representing complete condensate retention in the fully reversible limit. $\widehat{c_p}$ is the specific heat of the atmosphere per unit gaseous mole. Increases to the condensate loading of the atmosphere spread the energy required to change the temperature of the gas across a larger quantity of material without changing the amount of gas. This allows $\widehat{c_p}$ to exceed the specific heat capacity of either the gas or the condensate phases when the ratio of condensate to gas becomes large.

### 2.3. Adiabat Features

In order to illustrate the behavior of an atmospheric column described by the pseudoadiabat, we discuss the major features in a hypothetical $N_2$–$CO_2$–$H_2O$ atmosphere (Figure 1). Point 1 is the surface. Because we chose subsaturated surface conditions for all three gases, here the atmosphere follows the dry adiabatic lapse rate and the composition of the atmosphere does not change with height/pressure. This situation continues until the atmosphere intersects the local dew-point temperature of $H_2O$ ($T_{\text{dew}}(H_2O)$; depicted by the blue curve) at point 2, with the dew-point temperature approximated by (Pierrehumbert 2010)

$$T_{\text{dew}}(P) = \frac{T_0}{1 - \frac{RT_0}{L} \ln \frac{P}{P_{\text{sat}}(T_0)}}, \quad (37)$$

where $T_0$ is a reference temperature and the rest of the terms have been defined previously. For clarity, we note that this form of $T_{\text{dew}}$ assumes that the latent heat of vaporization is constant. This assumption was not used in the derivation of the pseudoadiabat in this paper.

Point 2 is the "cloud base" for $H_2O$; however, since we chose $\alpha = 0.0$, all condensate instantaneously rains out, so technically there would be no clouds in this particular atmospheric profile.

4

Above the cloud base, latent heat release from $H_2O$'s condensation decreases the lapse rate of the atmosphere by offsetting some of the cooling from expansion work.

Between points 2 and 3, the $H_2O$ in the column rains out and becomes a minor constituent of the atmosphere, with $CO_2$ replacing it as the dominant component. Point 3 is the $CO_2$ cloud base, where the pseudoadiabat crosses $CO_2$'s dew-point temperature. In general, an abrupt change to the pseudoadiabatic lapse rate in the figures in this paper signals the initiation of condensation for some species. Because $CO_2$ is by far the dominant gas in the atmosphere at this point (as $H_2O$ has rained out and $N_2$ is a minor background constituent), the pseudoadiabat essentially follows the $CO_2$ saturation vapor pressure curve above point 3 until it approaches point 4.

By point 4, most of the $CO_2$ in the atmosphere has rained out, leaving behind a tenuous upper atmosphere mostly consisting of $N_2$. The gradual bend in the profile that occurs at point 4 is due to a combination of the declining latent heat release as $CO_2$ becomes depleted and the smaller specific heat of $N_2$ ($\approx 29 \, J \, K^{-1} \, mol^{-1}$) compared to $CO_2$ ($\approx 36 \, J \, K^{-1} \, mol^{-1}$). A reduction in specific heat leads to a greater change in temperature for a given change in internal energy from expansion work done by the gas on its surroundings.

## 3. Case Studies

In this section we use the newly derived (pseudo)adiabat to model three nondilute atmospheres chosen to represent snapshots from the first billion years of the evolution of a terrestrial planet, demonstrating the broad utility of the formula and the potential importance of retained condensate fraction to atmospheric behavior. For a given profile, we use a single choice of $\alpha$ for all atmospheric species at all levels of the atmosphere, but it is important to note that in reality $\alpha$ would be determined by an intricate interplay of cloud microphysics and large-scale atmospheric dynamics, such that it would likely vary depending on the atmospheric constituent being considered and the position within the atmosphere. We use temperature-dependent specific heat capacities of gases and their liquid condensates from NIST (Lemmon et al. 2004). We do not account for solid condensates in our calculations, but they would be treated identically to liquids. We use constant latent heat values from Table 2.1 in Pierrehumbert (2010).

In addition to simulating different atmospheric profiles and compositions, we assess their radiative and spectral properties using the SOCRATES radiative transfer code (Edwards & Slingo 1996), solving the plane-parallel, two-stream approximated radiative transfer equation without scattering (cf. the more extensive description in Lichtenberg et al. 2021). Opacity coefficients are tabulated and derived from the HITRAN database (Gordon et al. 2017; Richard et al. 2012; Karman et al. 2019), making use of the line-by-line and collision-induced absorption coefficients for $H_2O$, $CO_2$, $H_2$ (Borysow et al. 2001; Borysow 2002), $CH_4$, $N_2$, and CO, as well as the $H_2O$ continuum (Mlawer et al. 2012).

### 3.1. Magma Ocean Exo-Earth during Planetary Assembly Phase

Terrestrial planets are thought to pass through an MO stage during their formation, with the planet's surface and interior rendered molten by the energy release from radionuclide decay and gravitational potential energy of the planet's constituent

mass (e.g., Elkins-Tanton 2012). The MO period is crucial in determining the initial atmosphere and climate of a terrestrial planet, and the composition of the atmosphere overlying an MO in turn exerts a primary control on the timescale of crystallization of the initially molten planetary mantle. MOs can also form later in the evolution of a planet, for example, after the planet goes through a runaway greenhouse event and accumulates a massive steam atmosphere.

The MO case demonstrates the control on cloud position exerted by the retained condensate fraction $\alpha$ via its influence on lapse rate (Figure 2). $H_2O$ makes up the lowest cloud deck, and the water cloud base occurs at the same point for all values of $\alpha$ (a pressure of several bars), since all three atmospheres follow the same dry adiabat in their respective noncondensing regions (panels (A1), (B1), (C1)).

In the $\alpha = 0.0$ case (Figure 2), no condensate remains in the column, so the specific heat per unit mole of gas in the atmosphere remains in the range $30-40 \, J \, K^{-1} \, mol^{-1}$ throughout (panel (A4)). This low specific heat allows for rapid cooling as pressure decreases, particularly after the $H_2O$ has largely been rained out and its latent heat effect has become insignificant at pressures below $\approx 10^{-1}$ bars (panel (A2)). $CO_2$ then condenses at approximately $10^{-2}$ bars and becomes an increasingly minor constituent of the atmosphere at lower and lower pressures, with $H_2$ becoming by far the dominant species at the top of the atmosphere.

The $\alpha = 0.1$ case (Figure 2) is similar to the full-rainout case, but not identical. With 10% of condensed moles retained, the effective specific heat of the atmosphere begins to increase above $H_2O$'s cloud base. This reduces the atmospheric lapse rate and ultimately causes $CO_2$ to begin condensing at $10^{-3}$ bars. In other words, the retention of 10% of condensate leads to an order-of-magnitude reduction in the cloud-base pressure of $CO_2$. At the top of the atmosphere, the effective atmospheric specific heat of the $\alpha = 0.1$ case is approximately double that of the $\alpha = 0.0$ case.

In the limit of full retention ($\alpha = 1.0$, bottom row of Figure 2), the increase in specific heat per mole of gas due to condensate is more dramatic, with $\hat{c}_p$ reaching a value of $\approx 200 \, J \, K^{-1} \, mol^{-1}$ (panel (C4)). With such large specific heat, the lapse rate above $H_2O$'s cloud base is small enough that $CO_2$ never condenses, in contrast to the cases with smaller $\alpha$. This makes it clear that condensate retention in nondilute atmospheres influences not just the position of successive cloud layers but also their presence or absence.

It is also worth noting that regardless of the value of $\alpha$, $H_2$ is the dominant constituent at the top of the atmosphere in all three cases examined in this section (see the second column of Figure 3). This contrasts with the results of Ingersoll (1969), the foundational first study of runaway greenhouse-induced steam atmospheres, which demonstrated that, with $N_2$ as the background gas, $H_2O$ remains the dominant atmospheric constituent even up to high altitudes and low temperatures if it is the dominant constituent at the planetary surface (see Figure 2 in Ingersoll 1969). The abundance of upper-atmospheric $H_2O$ in the Ingersoll (1969) runaway greenhouse simulations leads to efficient $H_2O$ photodissociation and subsequent escape, implying efficient planetary desiccation. With hydrogen as the background noncondensable, an upper atmosphere composed mostly of hydrogen is produced by our simulations, such that the $H_2$ may act as a shield, protecting atmospheric $H_2O$ from photodissociation. Thus, steam atmospheres may last longer on runaway greenhouse planets with large
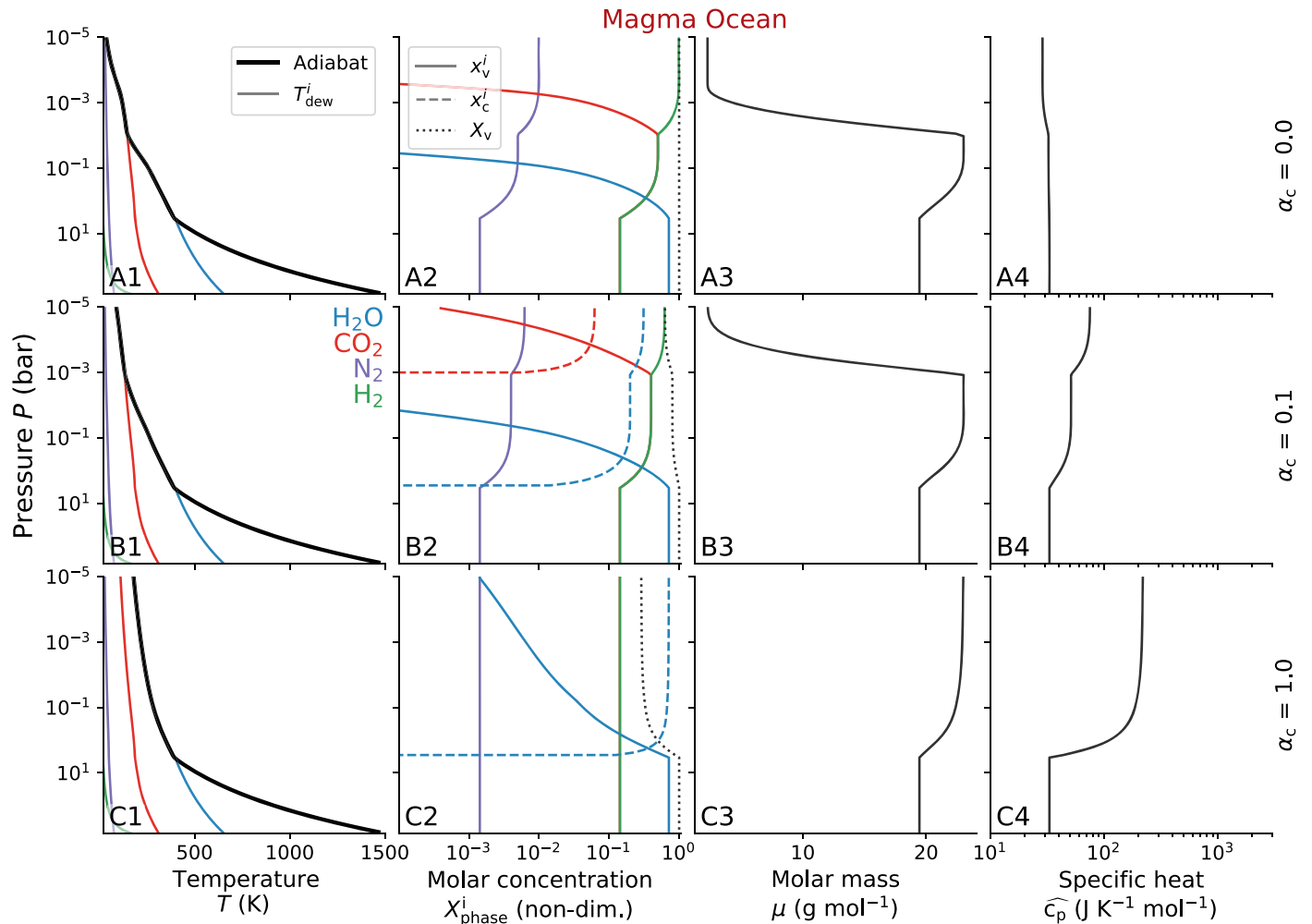
**Figure 2.** MO case study of a terrestrial planet with an inventory of about 1.85 Earth oceans (500 bars) $H_2O$, 100 bars $CO_2$, 100 bars $H_2$, and 1 bar $N_2$ in the atmosphere, with a surface temperature of 1500 K. The top row has retained condensate fraction $\alpha = 0$, the middle row has $\alpha = 0.1$, and the bottom row has $\alpha = 1$. We note here that the $\alpha = 1$ case, with full condensate retention, is unrealistic in atmospheres with nondilute condensable components and is included here as an illustration of the atmospheric profile produced by the condensate-retaining multicomponent moist adiabat derived in Li et al. (2018). The leftmost column shows the (pseudo)adiabat (thick black line) and the dew-point temperature of each component (thin colored lines), based on its partial pressure at a given atmospheric pressure. Varying the retained condensate fraction $\alpha$ from 0.0 to 0.1, and 1.0, substantially changes the lapse rate of the atmosphere and determines whether $CO_2$ condenses at all. The second column from the left displays the molar concentration of the different components of each atmosphere, including condensates when present. In the gaseous cases, $X_{phase}^i = \frac{x_{phase,i}}{1 - (1 - \alpha_i)x_{c,i}}$, while for the condensate, $X_c^i = \frac{\alpha_i x_{c,i}}{1 - (1 - \alpha_i)x_{c,i}}$. The third column from the left displays the average molar mass of the gaseous components of the atmosphere as a function of pressure. The rightmost column displays the atmospheric specific heat per unit mole of gas, $\hat{c}_p$ (defined below Equation (36)), as a function of pressure.

hydrogen inventories compared to those with large nitrogen inventories, since the planet's water will be destroyed more slowly, though it is also worth noting that the $H_2$ background gas would itself probably escape relatively quickly on these planets.

Clear-sky radiative transfer calculations for the MO atmospheres (Figure 4, left column) demonstrate substantial differences in outgoing radiation for the different $\alpha$ values (panel (A1)) and relatively minor changes to the spectrum of the radiation (panel (A2)). The top-of-atmosphere (TOA) outgoing radiation values are 159, 207, and 335 W m$^{-2}$ for the $\alpha = 0.0$, 0.1, and 1.0 cases, respectively. Thus, lapse rate changes from condensate retention can more than double the TOA outgoing radiation from an MO planet, though the inclusion of a stratosphere in radiative balance at the top of the atmosphere would likely reduce the contrast between the $\alpha = 1.0$ case and the other two cases, since the upper-atmospheric temperatures in the $\alpha = 0.0$ and 0.1 cases are unrealistically cold. Still, this suggests that the lapse rate changes caused by different condensate retention assumptions have

substantial influence on TOA outgoing radiation, with potentially important consequences for surface temperature and the timescale of MO crystallization, even without considering the (likely dominant) impact of clouds.

### 3.2. Hadean-analog Exo-Earth after a Major Late Veneer Impact

This planetary configuration is meant to represent an analog to a hot, chemically complex, transiently reducing atmosphere catalyzed by iron delivered to Earth's surface by the disrupted core of a Vesta-sized impactor during the LV on Hadean Earth (Genda et al. 2017; Benner et al. 2020; Zahnle et al. 2020). Impact-induced reducing atmospheres of this type have recently been hypothesized to have played a central role in the origin of life on Earth by allowing for the efficient creation of RNA precursors (Benner et al. 2020; Zahnle et al. 2020). The specific composition of this atmosphere (see Table 1) was drawn from Figure 3 in Zahnle et al. (2020), with an additional
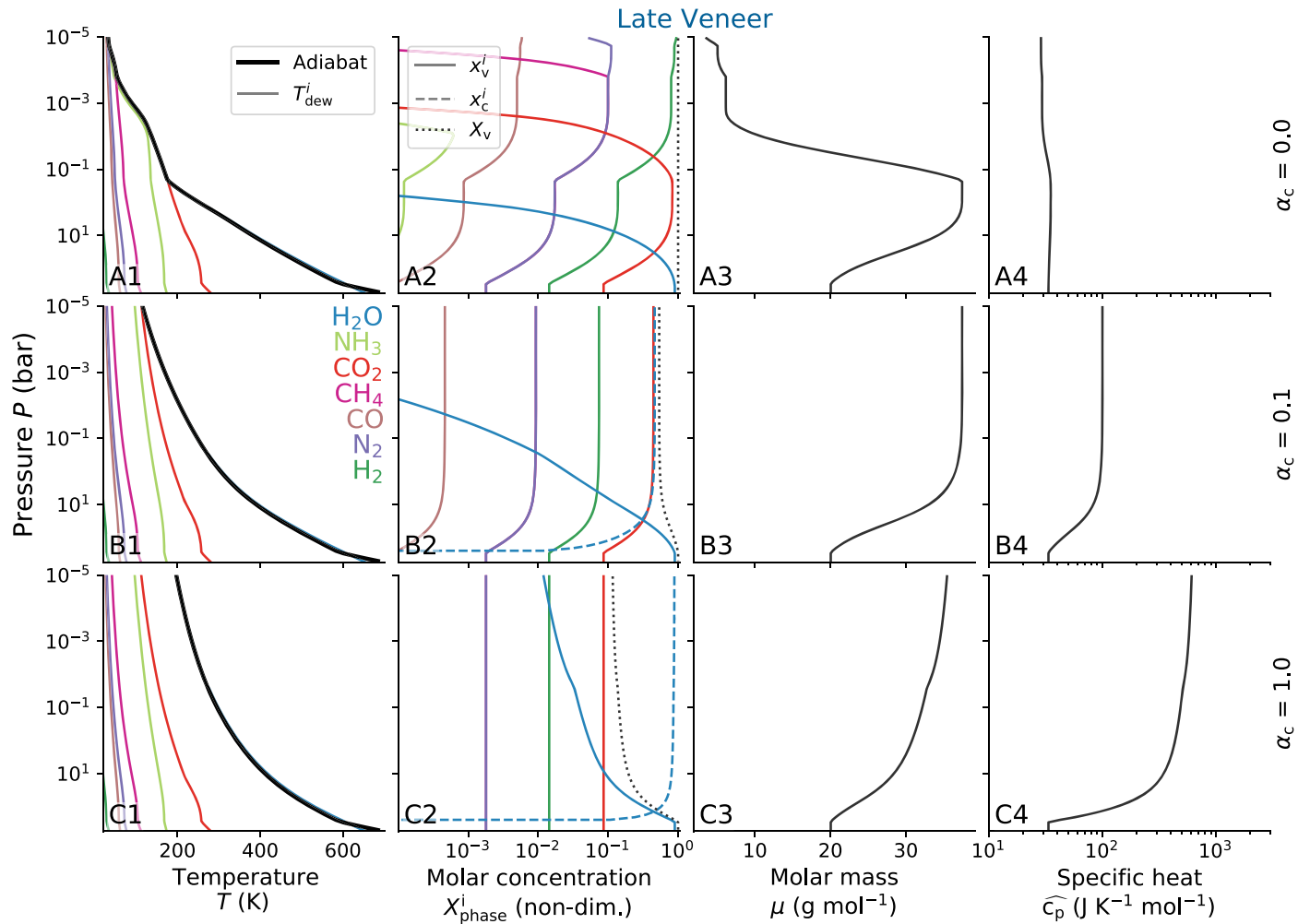
**Figure 3.** LV case study of a terrestrial planet after the impact of a reduced Vesta-sized body with an inventory of 500 bars $H_2O$, 48 bars $CO_2$, 8 bars $H_2$, 1 bar $N_2$, 1 bar $CH_4$, 0.05 bars CO, and 0.007 bars $NH_3$ in the atmosphere, with a surface temperature of 700 K. The top row has retained condensate fraction $\alpha = 0$, the middle row has $\alpha = 0.1$, and the bottom row has $\alpha = 1$. The leftmost column shows (pseudo)adiabat (thick black line) and the dew-point temperature of each component (thin colored lines), based on its partial pressure at a given atmospheric pressure. Varying the retained condensate fraction $\alpha$ from 0.0 to 0.1, and 1.0, substantially changes the lapse rate of the atmosphere and determines whether $CO_2$, $CH_4$, and $N_2$ condense at all. The second column from the left displays the molar concentration of the different components of each atmosphere, including condensates when present. In the gaseous cases, $X^i_{\text{phase}} = \frac{x_{\text{phase},i}}{1-(1-\alpha_i)x_{c,i}}$, while for the condensate, $X^i_c = \frac{\alpha_i x_{c,i}}{1-(1-\alpha_i)x_{c,i}}$. The third column from the left displays the average molar mass of the gaseous components of the atmosphere as a function of pressure. The rightmost column displays the atmospheric specific heat per unit mole of gas, $\widehat{c_p}$ (defined below Equation (36)), as a function of pressure.

500 bars of $H_2O$ to represent the $\approx 2$ oceans' worth of water that could have been vaporized by a Vesta-sized impactor (see Table 1 in Zahnle et al. 2020).

With full rainout ($\alpha = 0$, top row of Figure 3), four species condense at some point in the atmosphere: first $H_2O$ near the atmosphere's base, next $CO_2$ at approximately $10^{-1}$ bars, then $CH_4$ at $\approx 10^{-4}$ bars, and finally $N_2$ at $\approx 10^{-5}$ bars. In actuality, methane and nitrogen would probably not condense because radiative heating would likely warm the upper atmosphere to $>100$ K, but these calculations are meant to be illustrative. In any event, this sequence of condensations occurs because the lack of retained condensate allows the specific heat to remain at the low levels displayed by gaseous molecules without many internal degrees of freedom ($\approx 30$ J K$^{-1}$ mol$^{-1}$), forcing substantial cooling as the gas mixture ascends and expands.

In the $\alpha = 0.1$ (middle row of Figure 3) and $\alpha = 1.0$ (bottom row of Figure 3) cases, the specific heat per unit mole of gas reaches $\approx 100$ J K$^{-1}$ mol$^{-1}$ and $\approx 600$ J K$^{-1}$ mol$^{-1}$, respectively, as $H_2O$ condensates accumulate in the atmosphere. In

both of these cases, the high specific heat and correspondingly slow cooling of ascending parcels of air maintain the temperature above the condensation points of $CO_2$, $CH_4$, and $N_2$ throughout the atmosphere. In the $\alpha = 1$ case, the cooling with ascent is slow enough that gaseous $H_2O$ still makes up $\approx 1\%$ of the moles in the atmosphere at $10^{-5}$ bars (panel (B3)), while in the $\alpha = 0.1$ case the cooling is strong enough to reduce gaseous $H_2O$ to 0.01% of the moles in the atmosphere by $10^{-2}$ bars (panel (B2)). At pressures lower than about 100 bars, a majority of moles in the atmosphere of the $\alpha = 1$ case are condensed $H_2O$, and below 10 bars, the percentage approaches 99%.

The LV atmospheres display large differences in the TOA outgoing flux and spectral flux density at the three different $\alpha$ values considered (Figure 4, middle column). The outgoing flux values for the $\alpha = 0.0, 0.1$, and 1.0 cases are 38, 192, and 397 W m$^{-2}$, respectively (panel (B1)), an order-of-magnitude change between the limiting values. However, just like the MO case, it must be noted that a self-consistent stratosphere calculation would

**Table 1**
Case Study Reference Settings.

| Parameter | Unit | MO | LV | EE |
|---|---|---|---|---|
| $T_{surf}$ | K | 1500 | 700 | 290 |
| $pH_2O$ | bar | 500 | 500 | 0.01 |
| $pCO_2$ | bar | 100 | 48 | 29 |
| $pH_2$ | bar | 100 | 8 | ... |
| $pN_2$ | bar | 1 | 1 | 1 |
| $pCH_4$ | bar | ... | 1 | ... |
| $pCO$ | bar | ... | 0.05 | ... |
| $pNH_3$ | bar | ... | 0.007 | ... |

**Note.** MO: magma ocean; LV: late veneer; EE: exo-Earth.

markedly reduce this difference. Still, the potential changes in surface climate from changes to outgoing radiation of this magnitude are quite large and may be relevant to the prebiotic chemistry that has been suggested to occur in the aftermath of major LV impacts. There are also marked differences between the spectra of the LV variants (panel (B2)), with strong absorption lines in the 1–3 $\mu$m range present in the $\alpha = 1.0$ case but absent in the $\alpha = 0.1$ and 0.0 cases. This is because of the reduced concentration of $H_2O$ species in the colder upper atmospheres of the $\alpha = 0.0$ and 0.1 cases.

### 3.3. Archean-analog Exo-Earth near the Outer Edge of the Habitable Zone

Lastly, we consider a temperate (290 K) terrestrial planet with an atmosphere consisting of 29 bars of $CO_2$, 1 bar of $N_2$, and 0.01 bars of $H_2O$ at the surface (see Table 1 and Figure 5). Here, our Earth-like planet has passed through violent, rapidly evolving MO and LV stages and settled into a stable quasi-equilibrium, with high $pCO_2$ maintained by a carbonate-silicate cycle in response to relatively low insolation (e.g., Walker et al. 1981; Graham & Pierrehumbert 2020). This is an example of a hypothetical class of "habitable" planet that may exist near the outer edges of the liquid water habitable zones of some stars (e.g., Kopparapu et al. 2013). With such a high partial pressure, $CO_2$ in this atmosphere acts as a nondilute condensable component.

This impact of retained condensates on the effective atmospheric specific heat in this configuration is the strongest out of the three case studies. In the top row, where rainout is instantaneous and complete, the atmosphere has a specific heat of between 30 and 40 J K$^{-1}$ mol$^{-1}$ throughout (see panel (D1)). This causes the atmosphere to cool rapidly with height, particularly at pressures less than 10$^{-1}$ bars, where the $CO_2$ has mostly rained out (panel (B1)) and is no longer contributing a significant amount of latent heat. Since we do not account for upper-atmospheric radiative heating in the temperature profile, the gas mixture eventually grows so cold from expansion work that $N_2$ begins to condense at around 10$^{-3}$ bars. In actuality, the stratosphere would likely reach a temperature of around 150 K, given the $CO_2$-rich atmosphere and assumption of an outer-habitable-zone orbit (i.e., an insolation of something like 40% of Earth's; e.g., Kopparapu et al. 2013). This would certainly prevent the $N_2$ condensation in the $\alpha = 0$ case.

Shown in the middle row of Figure 5, condensate retention of 10% leads to nearly an order-of-magnitude increase in specific heat per mole of gas, with the atmosphere reaching $\approx$200 J K$^{-1}$ mol$^{-1}$ at $\approx$10$^{-1}$ bars (panel (D2)). Condensed $CO_2$ makes up a majority of the moles in the atmosphere at pressures lower than 10$^5$ Pa (panel (B2)). The $\alpha = 1.0$ case increases the specific heat of the

atmosphere by nearly another order of magnitude compared to the $\alpha = 0.1$ case, with $\hat{c}_p > 1000$ J K$^{-1}$ mol$^{-1}$ at pressures below 10$^{-1}$ bars (panel (D3)). This further slows the cooling with altitude, allowing $CO_2$'s partial pressure to fall more gradually compared to the $N_2$ partial pressure, such that the gaseous portion of the atmosphere is a mixture of those components in nearly equal parts at pressures lower than approximately 10$^{-1}$ bars (panel (B3)).

The radiative transfer differences for the three $\alpha$ variants of this case are smaller than in the MO and LV cases, though still large enough for potentially significant impacts on surface climate. The TOA outgoing radiation values for $\alpha = 0.0$, 0.1, and 1.0 are 81.1, 85.9, and 95.6 W m$^{-2}$, respectively. Similar to the MO and LV cases, the extremely cold temperatures reached in the upper atmosphere of the $\alpha = 0.0$ variant of this temperate, high-$pCO_2$ atmosphere are unrealistic because radiative balance would almost certainly establish a warmer stratosphere, which would lead to a greater value for TOA outgoing radiation. Still, differences of $\mathcal{O}(10$ W m$^{-2})$ can be significant for surface climate, with the potential to make the difference between a snowball state and a habitable state near the outer edge of the habitable zone. The differences in the spectra between the three $\alpha$ values for the EE case are mostly negligible, though there are order-of-magnitude differences between the $\alpha = 0.0$ and 1.0 cases between 6 and 10 $\mu$m.

### 4. Discussion

Improving our theoretical capabilities to model exotic atmospheres and compositional inventories of rocky planets is important for interpreting observations of extrasolar planets and further constraining the earliest planetary conditions of the terrestrial planets of the solar system, for which geochemical proxies are sparse. In this work we derived a novel, self-consistent prescription for the adiabatic lapse rate applicable to multicomponent, nondilute atmospheres on terrestrial worlds.

As demonstrated in Section 4, the changes in lapse rate and thus atmospheric temperature structure can have significant impacts on various aspects of the climate, from the spatial extent of condensing regions to molecular weight stratification, radiating properties, and spectral appearance. The changes for atmospheres with multiple nondilute condensable species described here may significantly alter the climate during important evolutionary epochs of planetary evolution. Therefore, the methodology presented here will in the future allow a better representation of these atmospheric features and pave the way to a more complete understanding of planetary evolution. In the following, we will discuss two different, but complementary, aspects of this work in more detail.

### 4.1. Implications for the Interpretation of Exoplanet Observations

Due to the observational bias in exoplanet detections, orbits within the runaway greenhouse limit are currently the dominant host of known rocky planets, such as super-Earths. Eclipse mapping techniques offer clues to the thermal and petrological properties of these extrasolar, terrestrial worlds (Demory et al. 2016; Kreidberg et al. 2019) and hold insights into the interaction of atmospheric constituents with underlying, potentially molten mantles. Upcoming ground- and space-based telescopes may enable us to directly image the light radiated from molten (Lupu et al. 2014; Bonati et al. 2019) and temperate (Morley et al. 2017; Quanz et al. 2019, 2021) extrasolar planets on wider orbits. Inverting these observations to infer atmospheric and, eventually,
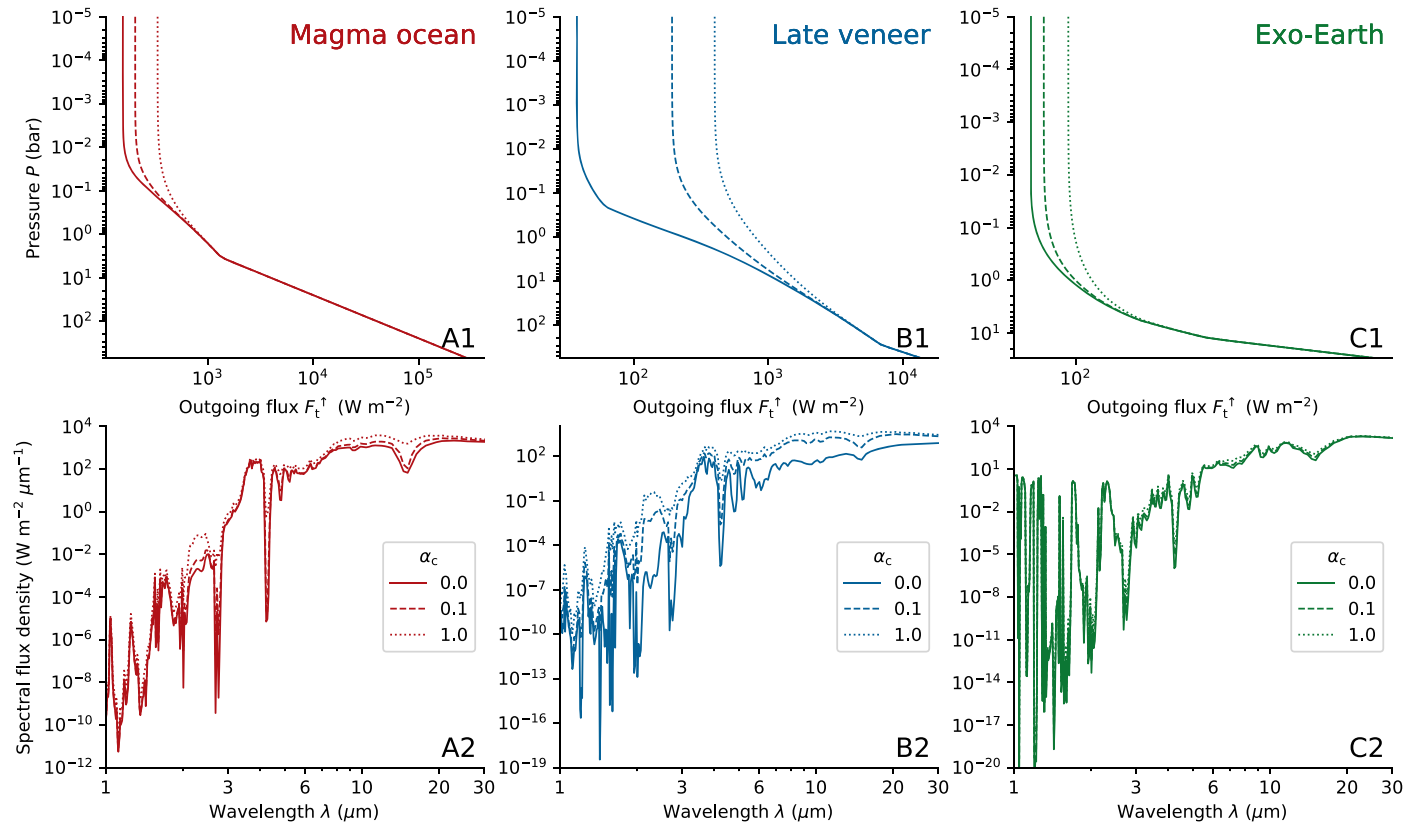
**Figure 4.** Deviations in planetary outgoing radiation and spectra for the three cases MO, LV, and EE, with varying condensate fraction $\alpha \in [0, 0.1, 1.0]$. All three cases show substantial changes in their outgoing radiation with $\alpha$, with the LV case changing by more than an order of magnitude. The MO and LV $\alpha$ variations differ in their spectra particularly at near- and mid-infrared wavelengths, most pronounced between 2 and 3 $\mu$m, and between $\approx$10 and 20 $\mu$m for the MO case and between $\approx$5 and 20 $\mu$m for the LV case. The EE $\alpha$ cases differ at $\approx$8 $\mu$m by up to one order of magnitude but are nearly indistinguishable elsewhere.

surface properties is sensitive to the underlying model assumptions. Because of the differences in temperature structure and related radiative and compositional properties, the pseudoadiabat derived in this work will enable more detailed reconnaissance of high molecular weight atmospheres and thus the transition from primary to secondary atmospheres (Kite & Barnett 2020).

In addition, because of the impact on thermal structure, $H_2O$ loss and abiotic generation of $O_2$-dominated atmospheres (Luger & Barnes 2015) through upper-atmosphere photolysis and subsequent escape can be affected by variations in retained condensate fraction. Our results here illustrate that variations on condensate retention may affect the $H_2$ abundances in the upper atmosphere, which can alter the degree of photodissociation and thus the lifetime of runaway greenhouse atmospheres on close-in rocky exoplanets. The amount of hydrogen loss in the upper atmosphere can be limited by the coldest region of the atmosphere (the cold trap; Wordsworth & Pierrehumbert 2013b). Therefore, in nondilute, high mean molecular weight atmospheres, deviations in tropopause location may impact the loss rate. Future work shall explore the link between outgassing speciation and retention from primordial evolutionary phases of rocky planets to more realistically capture this feedback between the planetary interior, atmospheric composition, and escape.

### 4.2. Implications for Early Earth Climate

A variety of different atmospheric compositions for early Earth have been suggested, in efforts to explain geochemical evidence for surface liquid water during the earliest epochs of

Earth's evolution (Mojzsis et al. 2001; Wilde et al. 2001) despite a faint young Sun, and to reconcile geochemical evidence for an oxidized mantle with the preference (Carlson et al. 2014; Armstrong et al. 2019) of prebiotic chemistry for reduced planetary environments (Benner et al. 2020; Sasselov et al. 2020). Hydrogen-rich environments have been suggested as promising solutions to both of these questions (Wordsworth & Pierrehumbert 2013a; Liggins et al. 2020) but were likely transient owing to the isotopic evidence for limited $p$H$_2$ after the Moon-forming giant impact (Pahlevan et al. 2019).

In this work we have shown the impact of our parameterization on the lapse rate for both the evolutionary cases of the more conservative $CO_2$-dominated early Earth atmosphere and the recently suggested, transiently reducing conditions due to LV impacts (Genda et al. 2017; Benner et al. 2020; Zahnle et al. 2020). The latter been suggested to exhibit a variety of complex atmospheric chemistries due to the dominant influence of iron rainout from the shredded impactor cores. During the following relapse of the atmosphere after such a catastrophic event, the near-surface conditions may intimately depend on the feedbacks between radiative structure and atmospheric chemistry, none of which can be adequately treated with simple single-species temperature structures.

Finally, even earlier, the creation of the primary atmosphere after MO cooldown is impacted by the redox state of the planetary interior and affects climate and atmospheric spectral appearance (e.g., Katyal et al. 2020). The MO cases shown in this work illustrate the impact on the cooling properties expected for such conditions, highlighting the
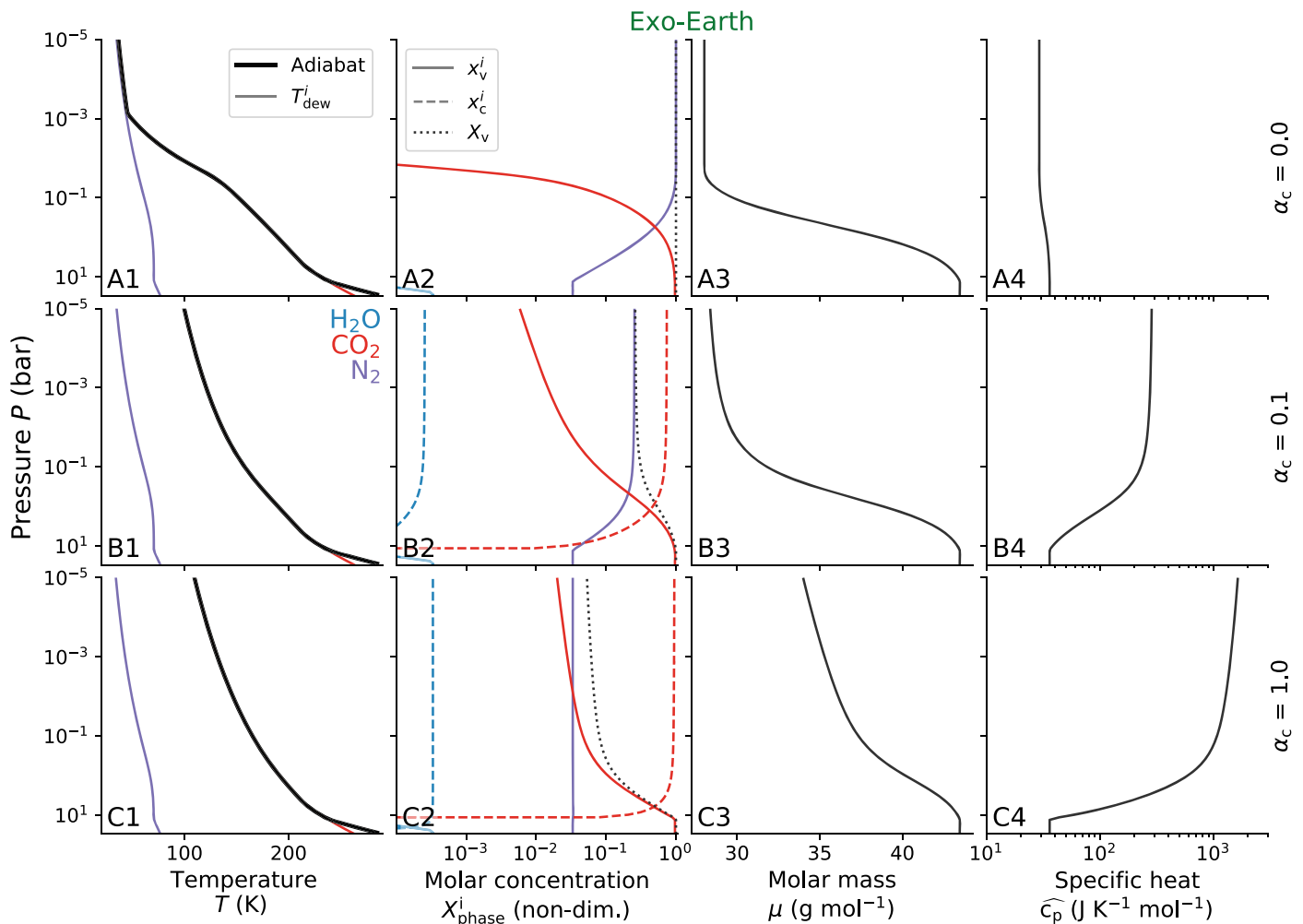
**Figure 5.** Exo-Earth (EE) case study of a terrestrial planet with 29 bars $CO_2$, 1 bar $N_2$, and 0.01 bars $H_2O$, with a surface temperature of 290 K. The top row has retained condensate fraction $\alpha = 0$, the middle row has $\alpha = 0.1$, and the bottom row has $\alpha = 1$. The leftmost column shows the (pseudo)adiabat (thick black line) and the dew-point temperature of each component (thin colored lines), based on its partial pressure at a given atmospheric pressure. Varying the retained condensate fraction $\alpha$ from 0.0 to 0.1, and 1.0, substantially changes the lapse rate of the atmosphere and determines whether $CO_2$ condenses at all. The second column from the left displays the molar concentration of the different components of each atmosphere, including condensates when present. In the gaseous cases, $X^i_{\mathrm{phase}} = \frac{x_{\mathrm{phase},i}}{1-(1-\alpha_i)x_{c,i}}$, while for the condensate, $X^i_c = \frac{\alpha_i x_{c,i}}{1-(1-\alpha_i)x_{c,i}}$. The third column from the left displays the average molar mass of the gaseous components of the atmosphere as a function of pressure. The rightmost column displays the atmospheric specific heat per unit mole of gas, $\widehat{c_p}$ (defined below Equation (36)), as a function of pressure.

need to appropriately account for multiple condensables under nondilute conditions to derive the earliest prebiotic planetary environment of the Hadean Earth.

### 4.3. Caveats

In the evaluation of the case studies presented in this paper, we neglected condensation-inhibited convection, cloud radiative effects, and the formation of a stratosphere, which, if included, could significantly impact some of the results. We discuss these phenomena in the following subsections.

#### 4.3.1. Condensation-inhibited Convection

Guillot (1995) and Leconte et al. (2017) demonstrated theoretically that the condensation of an atmospheric species with a molar mass higher than that of the noncondensing background gas can produce conditions that stabilize against convective and double-diffusive instability if the condensable is abundant enough. If this convective shutdown occurs where it is optically thick, energy flux through the

atmosphere is forced to proceed by radiative diffusion, resulting in sharp superadiabatic temperature gradients in the stabilized regions. This phenomenon can lead to hundreds-of-kelvin increases in the interior temperatures of solar system gas giants predicted by extrapolating from upper-atmospheric observations.

A number of the atmospheric compositions we consider in this study have condensable components that are of higher molar mass than their dry background components. This is clear when examining vertical stratification of molar mass in Figure 2 (panels (A3), (B3)), Figure 3 (panel (A3)), and Figure 5 (panels (A3), (B3), (C3)). In each of those cases, the average molar mass of the atmosphere substantially decreases with height owing to the condensation of a heavy, nondilute atmospheric component, and the concentrations of the condensables exceed the theoretical thresholds for inhibition of convection given by the formula presented in Guillot (1995) and Leconte et al. (2017). Just like in the gas giant cases explored in the original studies, this inhibition of convection should reduce the efficiency of the vertical transfer of energy

through the atmosphere, especially if the gradient in molar mass occurs in an optically thick region. Altering the lapse rate calculation in these regions to account for the dominance of radiative diffusion would lead to larger surface temperatures for a given level of outgoing radiation, in effect enhancing the greenhouse effect of these atmospheres. This effect could be important for the evolution of MOs and the climates of planets with thick $CO_2$–$N_2$–$H_2O$ atmospheres near the outer edges of liquid water habitable zones.

### 4.3.2. Cloud Impact on Radiative Transfer

In the radiative transfer calculations we carried out for this study, we neglected the impacts of clouds because of the complexities involved in self-consistently determining their properties in one-dimensional, steady-state models (e.g., Kopparapu et al. 2013). By definition, in all of the cases with $\alpha > 0$, clouds would in fact be present, so our neglect of cloud effects represents a significant simplification. The presence and position of cloud layers in terrestrial planetary atmospheres can have important impacts on both albedo (e.g., Yang & Abbot 2014; Pluriel et al. 2019) and outgoing radiation (e.g., Goldblatt & Zahnle 2011; Kitzmann 2016), in turn strongly affecting surface climate and the spectral signatures of atmospheres. With an assumed value for $\alpha$, the only additional information required to compute clouds' radiative impacts is the particle size distribution. Future work will assess the feedback between the radiative effects of clouds and the changes in lapse rate predicted by the formula derived in this work.

### 4.3.3. Formation of a Stratosphere

In the case studies, we neglected the formation of a stratosphere in radiative balance at the top of the atmosphere, instead focusing solely on the temperature–pressure profiles produced by the pseudoadiabat formula we derived. This leads to very cold temperatures at low pressures, particularly in the cases with $\alpha = 0.0$ or $0.1$. In actuality, absorption of stellar radiation at the top of the atmosphere would likely cause the atmosphere to display approximately isothermal or even increasing temperatures with height at low pressures, with details like the tropopause height and the cold trap temperature depending on the TOA installation, the spectrum of radiation received from the star, and the molecular species present. Under conditions with low installation and an atmosphere with abundant narrowband IR emitters like $CO_2$, frigid stratospheric temperatures are plausible. Higher installations or different compositions could lead to a warmer upper atmosphere, which would in some cases prevent condensation of species that condense when the atmosphere is modeled using only the pseudoadiabat. It would also increase outgoing radiation by allowing the upper atmosphere to emit larger quantities of thermal radiation, though the impact of this on surface climate should be modest (Pierrehumbert 2010). Still, without a formula that explicitly accounts for multiple nondilute condensing components, the influence of stratosphere formation on outgoing radiation and condensation in the upper atmosphere could not be self-consistently evaluated.

## 5. Conclusions

In this article, we derive a moist pseudoadiabatic lapse rate formula that allows for any number of condensables, each with arbitrary diluteness and arbitrary retained condensate fraction, and we apply the formula to a set of test cases to illustrate the behavior of terrestrial atmospheres with multiple condensable components and variable retained condensate fraction. The derivation is a generalization of that presented for the single-condensable case in Section 2.6.2 of Pierrehumbert (2010), and the formula is an expansion on the work of Li et al. (2018), which assumed full condensate retention. The introduction of an arbitrary retained condensate fraction is mainly useful for the modeling of atmospheres with nondilute condensable components, as a large fraction of a nondilute atmosphere's substance can be converted to solid or liquid condensate. The limit of complete condensate retention is probably unrealistic for atmospheres like this because of precipitation formation and dynamic instabilities from the negative buoyancy of condensate-rich layers. Applying the formula, we find the following:

1. Accounting for multiple condensing components with arbitrary retained condensate fraction produces an equation that is more complex than a simple linear superposition of single-component moist (pseudo) adiabats.
2. When condensate is retained in the nondilute limit, the effective specific heat per gaseous mole of an atmosphere can increase from tens of $J\,K^{-1}\,mol^{-1}$ to hundreds or even thousands of $J\,K^{-1}\,mol^{-1}$, strongly influencing the atmospheric lapse rate.
3. Changes to the atmospheric lapse rate can influence the position and presence of successive cloud layers in atmospheres with multiple condensables, the magnitude of the greenhouse effect, and the pressure at the base of the stratosphere.
4. The changes to condensate retention cause order-of-magnitude changes to the spectral flux density of outgoing radiation at a variety of wavelengths in all three atmospheric case studies.
5. In runaway greenhouse atmospheres where hydrogen acts as the background noncondensable, an upper atmosphere composed mostly of hydrogen may be produced. This suggests that $H_2$ can act as a shield to protect atmospheric $H_2O$ from photodissociation and hence prolong steam atmosphere lifetimes and increase water retention.
6. For young rocky planets in the MO phase or during Hadean-like early bombardment epochs, the spectral appearance in the near- to mid-infrared region can be affected by several orders of magnitude when varying the condensate retention fraction, though this ignores the undoubtedly significant impact of clouds on the spectrum.

The pseudoadiabat formula derived above enables more complete climate models to account for the effects of varying condensate retention in nondilute multicondensable atmospheres. Upcoming observations may make use of the newly derived formulation to calculate the detailed radiative–convective balance and infer near-surface properties of extrasolar rocky planets.

## ORCID iDs

R. J. Graham ⓘ https://orcid.org/0000-0001-9289-4416
Tim Lichtenberg ⓘ https://orcid.org/0000-0002-3286-7683
Ryan Boukrouche ⓘ https://orcid.org/0000-0002-5728-5129
Raymond T. Pierrehumbert ⓘ https://orcid.org/0000-0002-5887-1197

## References

Armstrong, K., Frost, D. J., McCammon, C. A., Rubie, D. C., & Boffa Ballaran, T. 2019, Sci, 365, 903
Benner, S. A., Bell, E. A., Biondi, E., et al. 2020, ChemSystemsChem, 2, e1900035
Bonati, I., Lichtenberg, T., Bower, D. J., Timpe, M. L., & Quanz, S. P. 2019, A&A, 621, A125
Borysow, A. 2002, A&A, 390, 779
Borysow, A., Jørgensen, U. G., & Fu, Y. 2001, JQSRT, 68, 235
Carlson, R. W., Garnero, E., Harrison, T. M., et al. 2014, AREPS, 42, 151
Demory, B.-O., Gillon, M., de Wit, J., et al. 2016, Natur, 532, 207
Ding, F., & Pierrehumbert, R. T. 2018, ApJ, 867, 54
Edwards, J. M., & Slingo, A. 1996, QJRMS, 122, 689
Elkins-Tanton, L. T. 2012, AREPS, 40, 113
Genda, H., Brasser, R., & Mojzsis, S. J. 2017, E&PSL, 480, 25
Goldblatt, C., & Zahnle, K. 2011, CliPa, 7, 203
Gordon, I. E., Rothman, L. S., Hill, C., et al. 2017, JQRST, 203, 3
Graham, R., & Pierrehumbert, R. 2020, ApJ, 896, 115
Guillot, T. 1995, Sci, 269, 1697
Ingersoll, A. 1969, J. Atmos. Sci., 26, 1191
Karman, T., Gordon, I. E., van der Avoird, A., et al. 2019, Icar, 328, 160
Katyal, N., Ortenzi, G., Lee Grenfell, J., et al. 2020, A&A, 643, A81
Kite, E. S., & Barnett, M. 2020, PNAS, 117, 18264
Kitzmann, D. 2016, ApJL, 817, L18
Kopparapu, R. K., Ramirez, R., Kasting, J. F., et al. 2013, ApJ, 765, 131
Kreidberg, L., Koll, D. D. B., Morley, C., et al. 2019, Natur, 573, 87
Leconte, J., Selsis, F., Hersant, F., & Guillot, T. 2017, A&A, 598, A98
Lemmon, E., McLinden, M., Friend, D., Linstrom, P., & Mallard, W. 2004, in NIST Standard Reference Database Number 69, ed. P. J. Linstrom & W. G. Mallard (Gaithersburg, MD: NIST)
Li, C., Ingersoll, A. P., & Oyafuso, F. 2018, J. Atmos. Sci., 75, 1063
Lichtenberg, T., Bower, D. J., Hammond, M., et al. 2021, JGRE, 126, e06711
Liggins, P., Shorttle, O., & Rimmer, P. B. 2020, E&PSL, 550, 116546
Luger, R., & Barnes, R. 2015, AsBio, 15, 119
Lupu, R. E., Zahnle, K., Marley, M. S., et al. 2014, ApJ, 784, 27
Mlawer, E. J., Payne, V. H., Moncet, J. L., et al. 2012, RSPTA, 370, 2520
Mojzsis, S. J., Harrison, T. M., & Pidgeon, R. T. 2001, Natur, 409, 178
Morley, C. V., Kreidberg, L., Rustamkulov, Z., Robinson, T., & Fortney, J. J. 2017, ApJ, 850, 121
Pahlevan, K., Schaefer, L., & Hirschmann, M. M. 2019, E&PSL, 526, 115770
Pierrehumbert, R. T. 2010, Principles of Planetary Climate (Cambridge: Cambridge Univ. Press)
Pierrehumbert, R. T., & Ding, F. 2016, RSPSA, 472, 20160107
Pluriel, W., Marcq, E., & Turbet, M. 2019, Icar, 317, 583
Quanz, S. P., Absil, O., Angerhausen, D., et al. 2019, arXiv:1908.01316
Quanz, S. P., Ottiger, M., & Fontanet, E. 2021, arXiv:2101.07500
Richard, C., Gordon, I. E., Rothman, L. S., et al. 2012, JQRST, 113, 1276
Sasselov, D. D., Grotzinger, J. P., & Sutherland, J. D. 2020, SciA, 6, eaax3419
Walker, J. C. G., Hays, P. B., & Kasting, J. F. 1981, JGR, 86, 9776
Weidenschilling, S., & Lewis, J. 1973, Icar, 20, 465
Wilde, S. A., Valley, J. W., Peck, W. H., & Graham, C. M. 2001, Natur, 409, 175
Wordsworth, R., & Pierrehumbert, R. 2013a, Sci, 339, 64
Wordsworth, R. D., & Pierrehumbert, R. T. 2013b, ApJ, 778, 154
Yang, J., & Abbot, D. S. 2014, ApJ, 784, 155
Zahnle, K. J., Lupu, R., Catling, D. C., & Wogan, N. 2020, PSJ, 1, 11